Mon. Not. R. Astron. Soc. **372,** 1749–1754 (2006) doi:10.1111/j.1365-2966.2006.10987.x

The environmental dependence of galaxy clustering in the Sloan Digital Sky Survey

Ummi Abbas[1]★ and Ravi K. Sheth[2]★

[1]*Department of Physics & Astronomy, University of Pittsburgh, Pittsburgh, PA 15260, USA*
[2]*Department of Physics & Astronomy, University of Pennsylvania, Philadelphia, PA 19104, USA*

Accepted 2006 August 21. Received 2006 August 21; in original form 2006 January 18

ABSTRACT

A generic prediction of hierarchical clustering models is that the mass function of dark haloes in dense regions in the Universe should be top-heavy. We provide a novel test of this prediction using a sample of galaxies drawn from the Sloan Digital Sky Survey (SDSS). To perform the test, we compare measurements of galaxy clustering in dense and underdense regions. We find that galaxies in dense regions cluster significantly more strongly than those in less dense regions. This is true over the entire 0.1–30 Mpc pair separation range for which we can make accurate measurements. We make similar measurements in realistic mock catalogues in which the only environmental effects are those which arise from the predicted correlation between halo mass and environment. We also provide an analytic halo model based calculation of the effect. Both the mock catalogues and the analytic calculation provide rather good descriptions of the SDSS measurements. Thus, our results provide strong support for hierarchical models. They suggest that, unless care is taken to study galaxies at fixed mass, correlations between galaxy properties and the surrounding environment are almost entirely due to more fundamental correlations between galaxy properties and host halo mass, and between halo mass and environment.

Key words: methods: analytical – galaxies: formation – galaxies: haloes – dark matter – large-scale structure of Universe.

1 INTRODUCTION

The correlation between galaxy properties (morphology, star formation rates, luminosity, colour, etc.) and the surrounding environment has been the subject of extensive studies in the last few decades: dense environments are preferentially occupied by elliptical, red, luminous galaxies, whereas star formation rates are higher in less dense regions (Dressler 1980; Butcher & Oemler 1984; Norberg et al. 2001; Balogh et al. 2002; Norberg et al. 2002; Gomez et al. 2003; Hogg et al. 2004; Kauffmann et al. 2004; Berlind et al. 2005; Croton et al. 2005). In hierarchical models, this behaviour is expected to be a consequence of the fact that galaxies are surrounded by dark matter haloes, and the properties of haloes (mass, formation time, concentration, internal angular momentum, etc.) are correlated with their environments (Mo & White 1996; Lemson & Kauffmann 1999; Sheth & Tormen 1999; Gottloeber, Klypin & Kravtsov 2001; Sheth & Tormen 2002, 2004; Avila-Reese et al. 2005; Gao, Springel & White 2005; Wechsler et al. 2005; Harker et al. 2006).

Recently, we described how the clustering of galaxies can be used to test the assumption that the correlations between galaxy properties and their environments are *entirely* a consequence of the correlations between haloes and their environments (Abbas & Sheth 2005). This is a strong assumption which significantly simplifies interpretation of the observed luminosity dependence of galaxy clustering (e.g. Zehavi et al. 2005). It is also a standard assumption in current halo model descriptions of galaxy clustering (see Cooray & Sheth 2002, for a review). The main goal of this paper is to perform this test.

This paper is arranged as follows. In Section 2 we show how galaxy clustering depends on environment in the Sloan Digital Sky Survey (SDSS; Adelman-McCarthy et al. 2006). In particular, we measure the pair correlation function in redshift space, $\xi(s \mid \delta_s)$, for a range of environments δ_s, as well as the projected quantity, $w_{\rm p}(r_{\rm p} \mid \delta_s)$; the latter is free of redshift-space distortions. These measurements are compared with similar measurements in carefully constructed mock catalogues, and from an analytic calculation based on the halo model. In both the mocks and the analytic calculation, correlations between galaxy properties and environment are entirely a consequence of the correlation between galaxy properties and halo masses, and between halo mass and environment. We summarize our results in Section 3, where we also discuss some implications. Appendix A provides details of the analytical model, which generalizes our earlier (real space) work so that it can be used to model redshift-space measurements as well.

★E-mails: ummi@phyast.pitt.edu (UA); shethrk@physics.upenn.edu (RKS)

2 THE ENVIRONMENTAL DEPENDENCE OF CLUSTERING

To measure the environmental dependence of clustering, we must decide on a measure of the environment. Abbas & Sheth (2005) showed that the precise choice of environment is not particularly important, in the sense that different choices lead to quantitative but not qualitative differences. They used N_R, the number of galaxies in a sphere of radius R centred on a galaxy, as a measure of that galaxy's environment, and presented results for $R = 5$ and $8\,h^{-1}$ Mpc. Their analysis was performed in real space. Performing a similar analysis in redshift space is complicated because the environmental effect we would like to test is due to correlations between halo masses with the real-space density. Therefore, we must find a definition of density in redshift space which is as faithful as possible to that in real space.

Line-of-sight redshift-space distortions can make a sphere in real space appear very different in redshift space. For instance, around a spherically symmetric cluster there are two main effects: one is due to coherent infall around the centre of the cluster, which appears as a squashing effect along the line of sight in redshift space (Kaiser 1987). The second is the 'finger of God' effect which is due to the virial motions of galaxies within the cluster (de Lapparent, Geller & Huchra 1986). This shows up as an elongation of the cluster along the line of sight. The squashing effect is relatively small, producing effects of order unity or less, whereas the 'finger of God' distortions are more dramatic – elongations along the line of sight are typically about a factor of 10. Since clusters have radii of a Mpc or so, fingers of god can extend up to about 10 Mpc. Therefore, while counts in redshift-space spheres of radii $5\,h^{-1}$ Mpc are not expected to faithfully trace the counts in the corresponding real-space spheres, counts in spheres of radii $8\,h^{-1}$ Mpc, N_8 should be more similar. For this reason, in what follows we use N_8 as a measure of the environment of each galaxy. (If we wished to push to smaller scales, we could identify all the fingers of god, and then 'decompress' them, by rescaling the distances along the line of sight so that they have the same extent as across the line of sight, for example, Tegmark et al. 2004. But performing such a 'manicure' is beyond the scope of the present work.)

We use N_8 to divide the galaxy population into three equal-sized subsamples: the third with the largest values of N_8 are defined as being the dense subsample, and the third with the smallest values of N_8 are the underdense subsample. We then measure the correlation functions in these two subsamples.

Our strategy is to make such measurements in a volume-limited galaxy catalogue, so that selection effects are minimized. We then compare with similar measurements in realistic mock catalogues. Throughout, we show results for a flat Lambda cold dark matter model for which $(\Omega_0, h, \sigma_8) = (0.3, 0.7, 0.9)$ at $z = 0$. Here Ω_0 is the density in units of critical density today, the Hubble constant at the present time is $H_0 = 100\,h\,\mathrm{km\ s^{-1}\ Mpc^{-1}}$, and σ_8 describes the rms fluctuations of the initial field, evolved to the present time using linear theory, when smoothed with a top-hat filter of radius $8\,h^{-1}$ Mpc.

2.1 The SDSS galaxy sample

We perform our analysis on a volume-limited catalogue extracted from the SDSS DR4 data base (Adelman-McCarthy et al. 2006). We chose galaxies brighter than $M_r < -21$, to match the analysis of Zehavi et al. (2005), whose results we use below. The resulting catalogue contains about 75 000 objects with accurate angular positions and redshifts, where the number density is 0.001 17 $(h^{-1}\,\mathrm{Mpc})^{-3}$.

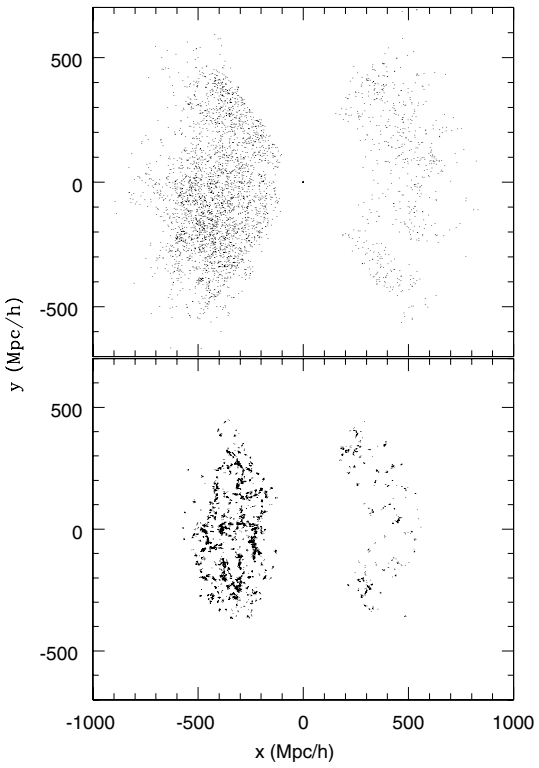

Figure 1. Pie diagrams of the SDSS subsamples: top and bottom panels show the distributions of objects classified as being in the least dense and the densest regions, in a slice of thickness $100\,h^{-1}$ Mpc through the survey volume.

As discussed above, we define the environment of each object using the redshift-space information. Fig. 1 shows the spatial distribution of galaxies in a thin slice through the SDSS volume-limited catalogue. Top panel shows the objects classified as being in the least dense regions, and bottom panel are for the objects in the densest regions. The galaxies in dense regions are clearly strongly clustered on small scales, whereas those in the underdense regions populate the holes defined by the spaces between the clusters that one sees in the dense sample.

The following sections quantify these differences by measuring the correlation functions in these subsamples. Uncertainties on our measurements were estimated by jack-knife resampling, in which the statistics were remeasured after omitting a random region, and repeated thirty times (approximately 1.5 times the total number of bins in separation for the results presented).

2.2 Mock galaxy samples

We have generated realistic mock galaxy samples as follows. We start with the Very Large Simulation (VLS; Yoshida, Sheth & Diaferio 2001), kindly made available to the public by the Virgo consortium. It has 512^3 particles in a cubic box with sides $L = 479\,h^{-1}$ Mpc. About 800 000 dark matter haloes, each containing at least 10 particles, were identified in this particle distribution using the Friends-of-Friends method. We use the simulation output for the mass, position and velocity of each dark matter halo.

We use the results of Zehavi et al. (2005) to motivate our choice for how mock galaxies should be distributed within each halo.

Specifically, to model a volume-limited galaxy catalogue with objects more luminous than L, haloes less massive than $m_{\rm L}$ are assumed to contain no galaxies; $m_{\rm L}$ depends on the galaxy population under consideration. Galaxies more massive than $m_{\rm L}$, contain one central galaxy, and may also contain satellite galaxies. The number of satellites is drawn from a Poisson distribution with mean $\langle N_{\rm s} \mid m\rangle$, where

$$\langle N_{\rm s} \mid m\rangle = \left(\frac{m}{m_1}\right)^{\alpha} \qquad \text{if } m \geqslant m_{\rm L}. \tag{1}$$

For SDSS galaxies more luminous than $M_{\rm r} < -21$, $m_{\rm L} = 10^{12.72}\,h^{-1}\,{\rm M}_{\odot}$, $m_1 = 23m_{\rm L}$ and $\alpha = 1.39$ (Zehavi et al. 2005). [A Poisson distribution for the number of satellites is motivated by the work of Kravtsov et al. (2004).] We then assume that the satellites in a halo are distributed around the halo centre similarly to the dark matter (e.g. Navarro, Frenk & White 1997).

To model redshift-space effects, we must model the velocity vector of each mock galaxy. We do so by assuming that $v_{\rm gal} = v_{\rm halo} + v_{\rm vir}$, where $v_{\rm halo}$ is the halo motion provided by the simulation, and $v_{\rm vir}$ is obtained as follows. The central galaxy in a halo is assumed to be at rest with respect to the halo, so $v_{\rm vir} = 0$. The virial motions of satellite galaxies are modelled by assuming that haloes are isotropic, virialized, and isothermal with Maxwellian velocities around the halo centre. The one-dimensional velocity dispersion is $1000\,(r_{200}h/{\rm Mpc})/\sqrt{2}$, where r_{200} is the scale on which the enclosed mass is 200 times the critical density: $m = 200\bar{\rho}_{\rm crit}\,(4\pi r_{200}^3/3)$. Following results in Sheth & Diaferio (2001), we assume that this virial term is independent of local environment.

In the distant observer approximation, the position in redshift space is $s = x + v_x/H_0$, where x is the real-space coordinate in the x direction, v_x is the x component of the peculiar velocity and s is the redshift-space distance in the x direction. The y and z components of the position are unchanged. The isothermal Maxwellian assumption means that the virial motions add Gaussian noise to the line-of-sight position of each satellite galaxy.

We then measure N_8 for each galaxy by counting the total number of galaxies within $8\,h^{-1}$ Mpc. For the mock catalogue, we can do this in both real and redshift space. Fig. 2 compares these two estimates of the local density. They are not widely different, suggesting that the analysis in Appendix A will be useful.

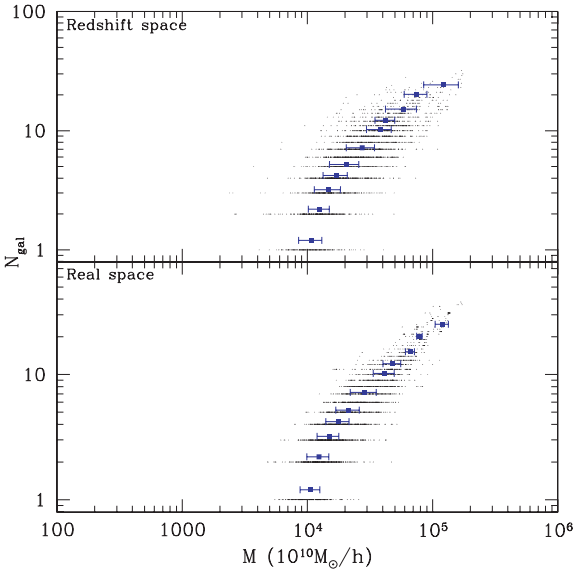

Figure 2. Comparison of local density estimates within real (bottom) and redshift (top) space spheres of radius $8\,h^{-1}$ Mpc. The median (given by the squares) and quartile range of halo mass corresponding to certain number of galaxies is shown (for clarity these points have been shifted upwards).

2.3 Results

Fig. 3 quantifies the spatial differences seen in Fig. 1; it shows the redshift-space correlation functions in dense and underdense regions measured in the mock catalogues (upper panel) and in the SDSS volume-limited catalogue (lower panel). In both panels, $\xi(s \mid \delta_s)$ for the dense sample is significantly larger than it is in the underdense sample. On large scales, this is because dense regions host the most massive haloes which in turn contain many galaxies; on smaller scales, the fact that the halo density profiles depend on halo mass also matters (Abbas & Sheth 2005). The inflection or break at the scale on which we define the environment ($8\,h^{-1}$ Mpc), which is seen in the clustering signal for underdense regions, arises because this scale is significantly larger than the virial radius of a typical halo. Let R denote the scale on which the environment is defined. Then, pairs which come from different haloes are of two types: those separated by scales smaller than R are said to be in the same patch, whereas more widely separated pairs are in different patches. Abbas & Sheth (2005) called these the $2h{-}1p$ and $2h{-}2p$ contributions to the statistic. Now, by definition, there are no $2h{-}2p$ pairs with separations smaller than $8\,h^{-1}$ Mpc, so $\xi_{2h-2p} = -1$ on smaller scales. In addition, underdense regions are those with small N_R, so they have few pairs in the $2h{-}1p$ term by definition. In the limit in which there is only one halo in each underdense patch (i.e. the one surrounding the galaxy around which the patch was centred),

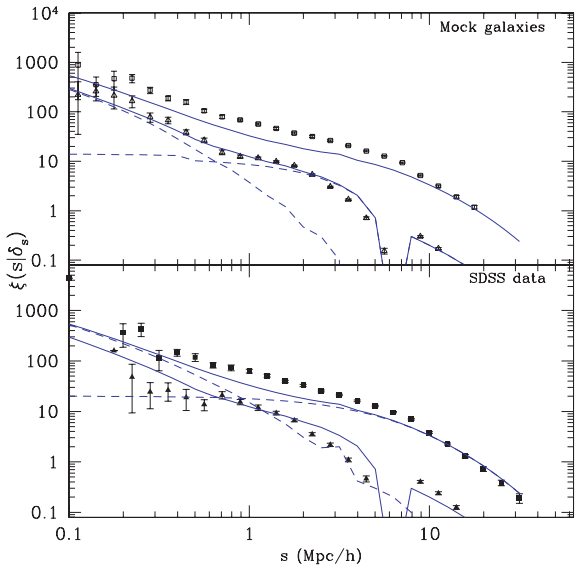

Figure 3. Environmental dependence of the galaxy correlation function in redshift space. Upper panel shows measurements in the mock catalogue, and lower panel shows measurements in the SDSS. In both cases, the galaxy catalogue is volume limited to $M_{\rm r} < -21$, and the environment of a galaxy was defined by counting the number of galaxies within a redshift-space sphere of radius $8\,h^{-1}$ Mpc centred on it. The squares and triangles in each panel show $\xi(s \mid \delta_s)$ for the galaxies in the densest 1/3 and least dense 1/3 of the sample. Solid curves show the analytic model for $\xi(s \mid \delta_s)$ that is developed in Appendix A. Dashed curves in the upper panel show the one-halo (dominates on small scales) and the sum of the $2h{-}1p$ and $2h{-}2p$ contributions (dominate on intermediate and large scales, respectively) to $\xi(s \mid \delta_s)$ of the less dense sample. In the lower panel, the dashed curves show these contributions for the dense sample.

there will be no $2h-1p$ pairs. In this limit, the correlation function is the sum of the $1h$ term, which falls rapidly on scales larger than the virial radius (a few Mpc) and the $2h$–$2p$ term (which is only significant on scales larger than the patch radius). Therefore, in this limit, if R is significantly larger than the virial radius of a typical halo, there will be a dramatic feature in ξ at scale R. As the number of $2h$–$1p$ pairs increases, this feature becomes less obvious. Indeed, in dense regions – those which have larger N_R and so have more $2h$–$1p$ pairs, there is little evidence of this feature.

The solid curves in the two panels show the analytic calculation outlined in the Appendix. They provide a reasonable description of the measurements in both panels. However, while the agreement is good on large scales, the curves underestimate the small-scale signal in dense regions. Since these smaller scales are the ones most affected by 'finger of God' distortions, it may be that the discrepancy is due to inadequacies in the analytic treatment of redshift-space effects (see Scoccimarro 2004, for a discussion of the sorts of effects our analysis ignores).

To eliminate this source of uncertainty, we have also studied the projected quantity

$$w_{\rm p}(r_{\rm p}\,|\,\delta_s) = 2\int_0^\infty {\rm d}\pi\,\xi(r_{\rm p},\pi\,|\,\delta_s), \qquad (2)$$

where $r = \sqrt{r_{\rm p}^2+\pi^2}$. We integrate up to $\pi = 35\,h^{-1}$ Mpc, which is large enough to include most correlated pairs. Fig. 4 shows the results, both in the mock catalogue (top panel) and in the SDSS (bottom panel). Now, the agreement with the analytical model is very good, suggesting that our analytic treatment of redshift-space distortions is inadequate. Once again, the inflection at the scale of the patch size for the underdense sample is caused due to the transition from one type of two-halo term to the other.

Both for $\xi(s\mid\delta_s)$ and $w_{\rm p}(r_{\rm p}\mid\delta_s)$ the differences between the two environments are dramatic – they are measured with high statistical significance. Nevertheless, the analytic model, which only incorporates those correlations with environment which arise from the correlation between halo mass and environment, provides an excellent description of the measurements. This leaves little room for other environmental effects.

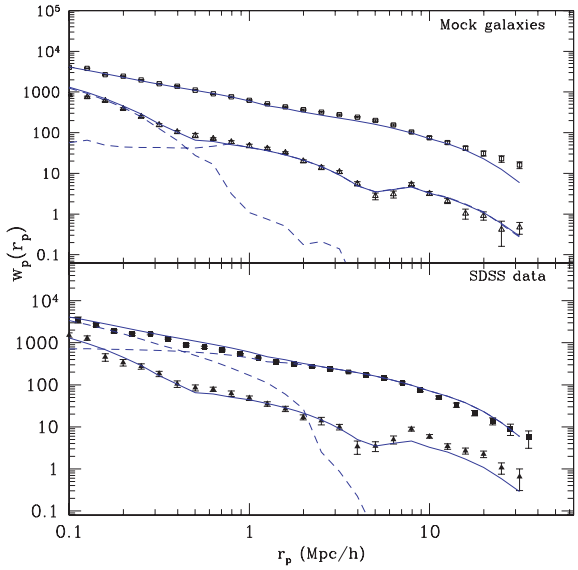

Figure 4. Similar to Fig. 3, but now for the projected galaxy correlation function. The upper panel shows measurements in the mock catalogue, and the lower panel is for the SDSS. Symbols and line styles are the same as for Fig. 3.

3 DISCUSSION AND CONCLUSIONS

One of the luxuries of the latest generation of large-scale sky surveys is that they contain sufficiently many objects that one can study subsamples of galaxies divided up in various ways. Here, we have focused on the clustering of galaxies in a volume-limited sample drawn from the SDSS, and studied how the clustering of these galaxies depends on environment. We find that galaxies in dense regions are considerably more strongly clustered than those in less dense regions (Figs 3 and 4).

This is perhaps not so surprising – after all, a dense region is one in which many galaxies are crowded together. What is more surprising is that this dependence on environment is very well reproduced by numerical (Section 2.2) and analytic (Appendix A) models in which the entire effect is due to the fact that galaxy properties correlate with the masses of their parent haloes, and massive haloes preferentially populate dense regions. Hierarchical models make quantitative predictions for this correlation between halo mass and environment, and so the agreement between our models and the measurements provides strong support for such models. In this respect, our results are consistent with those of Mo et al. (2004), Kauffmann et al. (2004), Berlind et al. (2005), Blanton et al. (2006) and Skibba et al. (2006); this is reassuring, since our methods are very different.

Our test of environmental effects is particularly interesting in view of recent work showing that, at fixed mass, haloes in dense regions form earlier (Sheth & Tormen 2004), and that this effect is stronger for low-mass haloes (Gao et al. 2005; Wechsler et al. 2005; Harker et al. 2006). Such a correlation is not part of our analytic model, nor is it included in our mock catalogues. Presumably, the good agreement with the SDSS measurements is due to the fact that we have concentrated on luminous galaxies, and these populate the more massive haloes. It will be interesting to see if this agreement persists at lower luminosities.

The agreement between our models and the measurements has an important consequence. Unless care is taken to study a population at fixed halo mass, our results indicate that observed correlations between astrophysical effects (e.g. ram-pressure stripping, strangulation, harassment) and environment are dominated by the fact that these effects also correlate with halo mass, and halo mass correlates with environment.

Larger samples will allow us to study if these trends persist to fainter, presumably less massive galaxies. And more distant samples will allow us to study if these trends evolve.

ACKNOWLEDGMENTS

We thank Ramin Skibba for many helpful discussions, Cameron McBride and Jeff Gardner for the NTROPY code which was used to measure the correlation functions and projected statistics in the simulations and data, Andrew Connolly and Ryan Scranton for providing the SDSS data samples used in this paper, and the Virgo consortium for making their simulations available to the public. We also thank the referee for suggesting changes that helped to improve the paper.

Funding for the SDSS has been provided by the Alfred P. Sloan Foundation, the Participating Institutions, the National Aeronautics and Space Administration, the National Science Foundation, the US Department of Energy, the Japanese Monbukagakusho and the Max Planck Society. The SDSS Web site is http://www.sdss.org/.

The SDSS is managed by the Astrophysical Research Consortium (ARC) for the Participating Institutions. The Participating Institutions are The University of Chicago, Fermilab, the Institute for Advanced Study, the Japan Participation Group, The Johns Hopkins University, the Korean Scientist Group, Los Alamos National Laboratory, the Max-Planck-Institute for Astronomy (MPIA), the Max-Planck-Institute for Astrophysics (MPA), New Mexico State University, University of Pittsburgh, University of Portsmouth, Princeton University, the United States Naval Observatory and the University of Washington.

REFERENCES

Abbas U., Sheth R. K., 2005, MNRAS, 364, 1327
Adelman-McCarthy J. K. et al., 2006, ApJS, 162, 38
Avila-Reese V., Colin P., Gottloeber S., Firmani C., Maulbetsch C., 2005, ApJ, 634, 51
Balogh M. L., Bower R. G., Smail I., Ziegler B. L., Davies R. L., Gaztelu A., Fritz A., 2002, MNRAS, 337, 256
Berlind A. A., Blanton M. R., Hogg D. W., Weinberg D. H., Dave R., Eisenstein D. J., Katz N., 2005, ApJ, 629, 625
Blanton M. R., Eisenstein D. J., Hogg D. W., Zehavi I., 2006, ApJ, 645, 977
Butcher H., Oemler A., 1984, ApJ, 285, 426
Croton D. J. et al., 2005, MNRAS, 356, 1155
Cooray A., Sheth R. K., 2002, Phys. Rep., 372, 1
Davis M., Peebles P. J. E., 1983, ApJ, 267, 465
de Lapparent V., Geller M. J., Huchra J. P., 1986, ApJ, 302, L1
Dressler A., 1980, ApJ, 236, 351
Gao L., Springel V., White S. D. M., 2005, MNRAS, 363, L66
Gomez P. L. et al., 2003, ApJ, 584, 210
Gottloeber S., Klypin A., Kravtsov A. V., 2001, ApJ, 546, 223
Harker G., Cole S., Helly J., Frenk C., Jenkins A., 2006, MNRAS, 367, 1039
Hogg D. W. et al., 2004, ApJ, 601, L29
Kaiser N., 1987, MNRAS, 227, 1
Kauffmann G. et al., 2004, MNRAS, 353, 713
Kravtsov A., Berlind A. A., Wechsler R. H., Klypin A. A., Gottloeber S., Allgood D. B., Primack J. R., 2004, ApJ, 609, 35
Lemson G., Kauffmann G., 1999, MNRAS, 302, 111
Mo H. J., White S. D. M., 1996, MNRAS, 282, 347
Mo H. J., Yang X., van den Bosch F. C., Jing Y. P., 2004, MNRAS, 349, 205
Navarro J. F., Frenk C. S., White S. D. M., 1997, ApJ, 490, 493
Norberg P. et al., 2001, MNRAS, 328, 64
Norberg P. et al., 2002, MNRAS, 332, 827
Scoccimarro R., 2004, Phys. Rev. D, 70. 3007
Seljak U., 2001, MNRAS, 325, 1359
Sheth R. K., 1996, MNRAS, 279, 1310
Sheth R. K., Diaferio A., 2001, MNRAS, 322, 901
Sheth R. K., Tormen G., 1999, MNRAS, 308, 119
Sheth R. K., Tormen G., 2002, MNRAS, 329, 61
Sheth R. K., Tormen G., 2004, MNRAS, 350, 1385
Skibba R., Sheth R. K., Connolly A. J., Scranton R., 2006, MNRAS, 368, 68
Tegmark M. et al., 2004, ApJ, 606, 702
Wechsler R. H., Zentner A. R., Bullock J. S., Kravtsov A. V. 2005, ApJ, submitted, preprint (astro-ph/0512416)
White M., 2001, MNRAS, 321, 1
Yoshida N., Sheth R. K., Diaferio A., 2001, MNRAS, 328, 669
Zehavi I. et al., 2005, ApJ, 630, 1

APPENDIX A: THE ANALYTICAL MODEL

This appendix discusses how the halo model calculation of environmental effects on clustering can be extended to include redshift-space effects. Our strategy is to combine the halo model description of redshift-space effects (Seljak 2001; White 2001) with the halo model description of environmental effects provided by Abbas & Sheth (2005).

In redshift space, two effects modify the real-space expressions derived by Abbas & Sheth (2005). One of these is a boost of power on large scales due to the instreaming of matter into overdense regions (Kaiser 1987); this affects the two-halo terms. Using density conservation to linear order and making the distant observer approximation, the redshift-space galaxy density perturbation can be written as

$$\delta_{\rm g}^{\rm rs} = \delta_{\rm g} + \delta_{\rm v}\mu^2 \tag{A1}$$

where $\mu = \hat{r}\hat{k}$, $\delta_{\rm g}$ is the real-space galaxy density perturbation and $\delta_{\rm v}$ is the velocity divergence. This is related to the density perturbation $\delta_{\rm dm}$ via $\delta_{\rm v} = f\delta_{\rm dm}$, where $f(\Omega) \equiv {\rm d}\log\delta/{\rm d}\log a \simeq \Omega^{0.6}$, and a is the scalefactor.

The other effect is the suppression of power due to the virial motions within haloes; this affects the one-halo term (Sheth 1996). The assumption of isotropic, isothermal, Maxwellian motions within haloes means that the effect can be modelled as a convolution with a Gaussian. In particular, the density contrast in redshift space is

$$\delta_{\rm g}^{\rm rs} = \delta_{\rm g}{\rm e}^{-(k\sigma\mu)^2/2}. \tag{A2}$$

Scoccimarro (2004) discusses why these descriptions (equations A1 and A2) of redshift-space distortions are rather crude. For our purposes, they represent reasonable first approximations to a more sophisticated model.

Let $n(M, V)$ denote the number density of patches of mass M and volume V, and let $N(m \mid M, V)$ be the average number of m haloes in regions of volume V which contain mass M. The isotropized redshift-space power spectrum is obtained by averaging $(\delta_{\rm g}^{\rm rs})^2$ over μ, m and M. In particular, the one-halo term can be written as

$$P_{1h}^{\rm gal}(k \mid \delta) = \int_{M_{\rm min}}^{M_{\rm max}} {\rm d}M\, n(M, V) \int_0^M {\rm d}m\, N(m \mid M, V) \times \frac{\left[\langle 2N_{\rm s} \mid m\rangle\, u(k \mid m)\Re_1(k\sigma) + \langle N_{\rm s} \mid m\rangle^2\, |u(k \mid m)|^2\Re_2(k\sigma)\right]}{\bar{n}^2_{\delta-{\rm gal}}}, \tag{A3}$$

where

$$\Re_{\rm p}(\alpha = k\sigma[p/2]^{1/2}) = \frac{\sqrt{\pi}}{2}\frac{{\rm erf}(\alpha)}{\alpha} \tag{A4}$$

for $p = 1,\ 2$, and $\bar{n}_{\delta-{\rm gal}}$ is the number density of galaxies surrounded by regions containing at least $N_{\rm min}$ other galaxies:

$$\bar{n}_{\delta-{\rm gal}} = \int_{M_{\rm min}(N_{\rm min})}^{M_{\rm max}(N_{\rm max})} {\rm d}M\, n(M, V) \times \int_0^M {\rm d}m\, N(m \mid M, V)\, \langle N_{\rm gal} \mid m\rangle. \tag{A5}$$

Here, $\langle N_{\rm gal} \mid m\rangle = 1 + \langle N_{\rm s} \mid m\rangle$ is the average number of galaxies occupying a halo of mass m (in our model, it is zero below some $m_{\rm L}$; cf. equation 1). In practice, $M_{\rm min}(N_{\rm min})$ is obtained by varying $N_{\rm min}$ until the value of this expression matches the observed number density.

The two-halo term is more complex as it now has two types of contributions: pairs which are in the same patch ($2h$–$1p$), and pairs in different patches ($2h$–$2p$). The $2h$–$1p$ term can only be important on intermediate scales (i.e. those which are larger than the diameter of a typical halo but smaller than the diameter of a patch). The $2h$–$2p$

term is

$$P^{\rm gal}_{2h-2p} = \left(F_{\rm g}^2 + \frac{2}{3}F_{\rm v}F_{\rm g} + \frac{1}{5}F_{\rm v}^2\right) P_{\rm Lin}(k \mid R_{\rm p}), \tag{A6}$$

where

$$\begin{aligned} F_{\rm v} &= f \int_{M_{\rm min}}^{M_{\rm max}} {\rm d}M\, n(M, V)\, B(M, V) \\ &\quad \times \int_0^M {\rm d}m\, N(m \mid M, V)\, \frac{m}{\rho_\delta} \Re_1(k\sigma) u(k \mid m), \\ F_{\rm g} &= \int_{M_{\rm min}}^{M_{\rm max}} {\rm d}M\, n(M, V)\, B(M, V) \\ &\quad \times \int_0^M {\rm d}m\, N(m \mid M, V)\, \frac{\langle N_{\rm gal} \mid m\rangle}{\bar{n}_{\delta-{\rm gal}}} \Re_1(k\sigma) u(k \mid m). \end{aligned} \tag{A7}$$

$P_{\rm Lin}(k \mid R_{\rm p})$ denotes the power spectrum associated with setting the linear theory correlation function to -1 on scales smaller than the diameter of a patch $2R_{\rm p}$. This truncation has little effect on small $kR_{\rm p} \ll 1$, where $P_{\rm Lin}(k \mid R_{\rm p}) \approx P_{\rm Lin}(k)$. And the factor $B(M, V)$ describes the bias associated with the clustering of the patches; it depends on the abundance of such patches (see Abbas & Sheth 2005, for details).

Similarly, the $2h$–$1p$ term can be written as

$$\begin{aligned} P^{\rm gal}_{2h-1p}(k \mid \delta) &= \int_{M_{\rm min}}^{M_{\rm max}} {\rm d}M\, n(M, V) \left(F_{\rm g}'^2 + \frac{2}{3}F_{\rm v}'F_{\rm g}' + \frac{1}{5}F_{\rm v}'^2\right) \\ &\quad \times [P_{\rm Lin}(k) - P_{\rm Lin}(k \mid R_{\rm p})], \end{aligned} \tag{A8}$$

where $P_{\rm Lin}(k) - P_{\rm Lin}(k \mid R_{\rm p})$ denotes the power spectrum associated with setting the linear theory correlation function to zero on scales larger than the diameter of a patch $2R_{\rm p}$, and

$$\begin{aligned} F_{\rm v}' &= f \int_0^M {\rm d}m\, N(m \mid M, V)\, \frac{m}{\rho_\delta} \Re_1(k\sigma) b(m)\, u(k \mid m) \\ F_{\rm g}' &= \int_0^M {\rm d}m\, N(m \mid M, V)\, \frac{\langle N_{\rm gal} \mid m\rangle}{\bar{n}_{\delta-{\rm gal}}} \Re_1(k\sigma) b(m)\, u(k \mid m). \end{aligned} \tag{A9}$$

Here $b(m)$ is the bias factor of haloes of mass m (from Sheth & Tormen 1999). The correlation function, $\xi(s)$, is obtained by taking the Fourier transform of the power spectrum $P(k)$.

This paper has been typeset from a TEX/LATEX file prepared by the author.